Journal for ImmunoTherapy of Cancer

Sensitivity to immune checkpoint inhibitors in BRAF/MEK inhibitor refractory melanoma

Riyaben P Patel [1,2] Lydia Rui Jia Lim [1,2] Reem Saleh [1] Darius Schenk,[1] Michael K Lee,[1,2] Emily Lelliott,[3,4,5,6] Aparna D Rao [1,2] Shaghayegh Arabi,[1,2] Lorey Smith [1,2] Anna S Trigos [1,2] Nicole Haynes,[1,2] Grant A McArthur,[1,2] Karen E Sheppard [1,2]

To cite: Patel RP, Lim LRJ, Saleh R, *et al*. Sensitivity to immune checkpoint inhibitors in BRAF/MEK inhibitor refractory melanoma. *Journal for ImmunoTherapy of Cancer* 2025;**13**:e011551. doi:10.1136/jitc-2025-011551

► Additional supplemental material is published online only. To view, please visit the journal online (https://doi.org/10.1136/jitc-2025-011551).

GAM and KES are joint senior authors.

Accepted 28 April 2025

For numbered affiliations see end of article.

Correspondence to
Dr Karen E Sheppard;
karen.sheppard@petermac.org

ABSTRACT

Background Resistance to BRAF and MEK inhibitors (BRAFi/MEKi) in metastatic melanoma frequently results in cross-resistance to immune checkpoint inhibitors (ICI), limiting effective treatment options. However, a subset of BRAFi/MEKi-resistant patients remains responsive to second-line ICI, suggesting heterogeneous underlying resistance mechanisms. This study aimed to explore the tumor immune microenvironment in BRAFi/MEKi-resistant melanoma to uncover factors influencing sensitivity to second-line ICI therapy.

Method To investigate mechanisms underlying resistance and responsiveness to second-line ICIs, BRAFi/MEKi-resistant melanoma mouse models were used. Flow cytometry was employed to analyze immune cell populations within the tumor microenvironment, focusing on changes in CD8+T effector cells and other key immune subsets. RNA sequencing was performed to profile transcriptomic changes in resistant tumors, providing insights into the signaling pathways associated with resistance. Clinical samples from BRAFi/MEKi-resistant patients were further evaluated for correlations between immune profiles and key signaling pathways to support findings from the preclinical models.

Results Using BRAFi/MEKi-resistant melanoma mouse models, we observed distinct alterations in the tumor-immune microenvironment. Tumors exhibiting resistance showed a significant increase in CD8+T effector cells following BRAFi/MEKi treatment, suggesting an immune-stimulatory response. Mechanistic analysis identified the activation of the EGFR-STAT signaling pathway as a key driver of intrinsic resistance in these models. Notably, these tumors retained sensitivity to second-line ICI therapy, contrasting with NRAS-driven BRAFi/MEKi-resistant tumors, which demonstrated cross-resistance to ICIs. Supporting these findings, clinical samples from BRAFi/MEKi-resistant patients revealed a correlation between elevated EGFR activation and higher immune scores, indicating potential sensitivity to ICI therapy in this subset of patients.

Conclusion EGFR overexpression emerges as a potential predictive biomarker for responsiveness to second-line ICIs in BRAFi/MEKi-resistant melanoma. These findings underscore the need for stratified therapeutic approaches and highlight EGFR as a target for improving outcomes in ICI therapy.

WHAT IS ALREADY KNOWN ON THIS TOPIC

⇒ Resistance to BRAF/MEK inhibitors (BRAFi/MEKi) in metastatic melanoma often leads to cross-resistance to immune checkpoint inhibitors (ICIs), which is linked to overactivation of the mitogen-activated protein kinase (MAPK) pathway. However, not all patients acquire resistance via MAPK pathway overactivation, and a subset of patients remains responsive to second-line ICI.

WHAT THIS STUDY ADDS

⇒ This study identifies EGFR-STAT signaling as a key mechanism of BRAFi/MEKi resistance, with tumors showing increased CD8+T effector cells and responsiveness to second-line ICIs, unlike NRAS-driven resistant tumors.

HOW THIS STUDY MIGHT AFFECT RESEARCH, PRACTICE OR POLICY

⇒ These findings may inform the development of predictive biomarkers for ICI responsiveness and guide patient selection for second-line ICI therapy, potentially improving melanoma treatment strategies

INTRODUCTION

The development of targeted therapies (TT) directed at BRAF ((B-Raf Proto-Oncogene, Serine/Threonine Kinase) and MEK (Mitogen-activated protein kinase), and immune checkpoint inhibitors (ICI) has revolutionized the treatment landscape of metastatic cutaneous melanoma, significantly improving patient outcomes. Despite their success, both TT and ICI have their limitations. Specifically, the combination of BRAF and MEK inhibitors (BRAFi/MEKi) effectively suppresses the hyperactive Ras-Raf-MEK-ERK (Extracellular signal-regulated kinase) mitogen-activated protein kinase (MAPK/ERK) pathway, resulting in high initial response rates. However, these responses are often short-lived, with patients developing resistance within 1–2 years of starting

treatment.[1 2] In contrast, ICIs, such as anti-cytotoxic T lymphocyte antigen-4 (CTLA-4), anti-programmed cell death-1/programmed death-ligand-1 (PD-1/PD-L1) and anti-lymphocyte activation gene 3 (LAG-3), have been shown to induce more durable antitumor responses, though with lower overall response rates.[3]

Due to the distinct yet complementary mechanisms of actions of ICI and TT therapies, their use in combination has been explored.[4 5] Preclinical data have shown that BRAFi/MEKi alter the melanoma immune microenvironment,[6–9] likely making it more amenable to ICI. In recent clinical trials the combination of BRAFi/MEKi with anti-PD-1 promoted higher progression-free survival although with higher grade 3–4 toxicities.[10 11] To overcome toxicity concerns, the DREAMseq[12] and SECOMBIT[13] trials investigated optimal sequencing strategies for first-line therapy in patients with disease progression. Both studies evaluated whether initiating treatment with ICI followed by TT on progression would result in superior outcomes compared with starting with TT and switching to ICI. Findings from both trials demonstrated significantly improved overall survival with the ICI-first strategy (SECOMBIT: 62% vs 54%; DREAMseq: 66.2% vs 42.8%).[12 13] Although these findings support ICI as the preferred first-line treatment for patients with advanced BRAF mutant melanoma, BRAFi/MEKi treatment remains a clinically valuable option, particularly in cases where rapid tumor control is required. This includes patients with poor prognostic features such as high tumor burden, elevated Lactate Dehydrogenase (LDH) levels, or symptomatic brain metastases, where ICI may not be suitable as an immediate intervention.[14] In such scenarios, TT as first-line therapy followed by a transition to ICI once the disease burden is reduced is necessary. Therefore, to support treatment decisions during the transition to ICI, critical questions remain to be addressed. Specifically, what are the mechanisms by which TT induces cross-resistance to subsequent ICI therapy? Additionally, why do approximately 40% of patients treated with TT remain responsive to second-line ICI treatment? Addressing these questions and thereby identifying biomarkers of response and resistance are crucial for optimizing treatment strategies and improving patient outcomes.

Acquired resistance to BRAFi/MEKi in melanoma occurs in 70% of patients, often due to MAPK/ERK pathway reactivation.[15] This can involve either the upregulation/activation of positive regulators (eg, BRAF, MEK1, MEK2, NRAS) or the downregulation of negative regulators (eg, NF1).[16 17] Additionally, other contributing factors include overactivation of survival pathways such as PI3K-AKT, hyperactivation of receptor tyrosine kinases (RTKs) including Epidermal growth factor receptor (EGFR), Platelet-derived growth factor receptor beta (PDFRβ), Insulin-like Growth Factor 1 Receptor (IGF-1R), and Hepatocyte Growth Factor (HGF) receptor,[18–20] or dysregulation of Microphthalmia-associated transcription factor (MITF).[21] Tumor immune microenvironment changes, including reduced cytotoxic T-cell infiltration,[22] increased immunosuppressive T-regulatory cells,[9] and upregulation of immune exhaustion markers (eg, PD-1, T-cell immunoglobulin and mucin domain-containing protein 3 (TIM3)) also play a role.[8 9] These studies suggest that patients can develop resistance to TT through various mechanisms.[23] Therefore, models that simulate sensitivity or cross-resistance to ICI after BRAFi/MEKi resistance are needed to explore responses to second-line ICI.

Herein, we show tumors that develop resistance to BRAFi/MEKi via upregulated EGFR-signal transducer and activator of transcription (STAT) signaling maintain sensitivity to second-line ICI therapy. We reveal that while resistance to BRAFi/MEKi is evident in immune-compromised NSG mice, it manifests as partial sensitivity in immunocompetent C57BL/6 mice, suggesting that the immune system plays a critical role in modulating the response of these acquired resistant tumors. Analysis of the tumor immune microenvironment highlighted a significant increase in CD8+T effector cells following BRAFi/MEKi treatment in acquired resistant tumors compared with sensitive tumors. Importantly, BRAFi/MEKi-resistant and sensitive tumors exhibited responsiveness to both anti-CTLA-4 and anti-PD-1 therapy. Mechanistically, upregulation of the EGFR-STAT pathway in BRAFi/MEKi acquired resistant melanoma cells drives their proliferation in response to treatment. Clinical observations further supported our findings. We demonstrate that patients with elevated EGFR activity on BRAFi/MEKi progression exhibit significantly higher immune scores compared with those without such upregulation, suggesting potential sensitivity to ICI. Our study highlights the importance of understanding the mechanisms of resistance to TT to inform second-line ICI. Specifically, our findings strongly support EGFR overexpression as a potential biomarker for patient stratification to second-line immunotherapy. Moreover, our study lays the groundwork for elucidating why only a subset of patients respond favorably to second-line ICI treatment.

MATERIALS AND METHODS

Cell lines and in vitro drug assays

To obtain consistent *in vivo* growth of the YUMMER (YR) 1.7 cell line,[24] YR1.7 tumors were harvested from C57BL/6 mice and a cell line created named YR1.7 passage variant 1 (YR1.7PV1: online supplemental figure S1A,B). Tumors were processed by chopping and digesting with collagenase (1.6 mg/mL; Worthington Biochemical Corporation, Cat.no. LS004188) and DNase (2 U/mL; Merck, Cat.no. 11284932001) in Dulbecco's Modified Eagle's Medium (DMEM) + 2% Fetal bovine serum (FBS) for 45 min at 37°C under sterile conditions. The digested solution was filtered through 70 µm filters and cultured in antibiotic-antimycotic solution (Thermo Fisher Scientific, Cat. no. 15240062) for 3 weeks, resulting in the first batch of YR 1.7 PV1 cells. To induce resistance, YR1.7PV1 cells were cultured with increasing concentrations of dabrafenib and trametinib (BRAFi/

MEKi) for 46 passages (~6 months). Post-resistance acquisition, cells were maintained off drug pressure for routine use. All cell lines were cultured in Roswell Park Memorial Institute Medium (RPMI)-1640 medium supplemented with 10% FBS, 2 mM GlutaMAX (Thermo Fisher Scientific, Cat.no. 35050061), 1 mM sodium pyruvate (Thermo Fisher Scientific, Cat.no. 11360070), 1% non-essential amino acids (Thermo Fisher Scientific, Cat.no. 11140050), 50 µM β-mercaptoethanol, and buffered with HEPES (4-(2-Hydroxyethyl)-1-piperazineetha nesulfonic acid) (Merck, Cat.no. H0887). Cultures were maintained at 37°C in a 5% CO2 incubator and routinely tested for *Mycoplasma* contamination. For the proliferation assays and western blot analysis, cells were treated with dabrafenib (50–100 nM: MCE, cat. No. HY-14660A), trametinib (5–10 nM: MCE, cat no. HY-1099), 2 µM of erlotinib (EGFRi) (MCE, cat no. HY-50896), 200 nM of napabucasin (STAT3i: Cat. no. HY-13919), 1 µM of AC-4–130 (STAT5i: MCE, cat no. HY-124500) and 2 µM of ruxolitinib (MCE, cat no. HY-50856). DMSO (Dimethyl sulfoxide) was used as a vehicle for all in vitro drug assays.

Animal models, in vivo growth and therapy studies

Animal experiments followed National Health and Medical Research Council guidelines and received approval from the Peter MacCallum Animal Experimentation Ethics Committee. Male C57BL/6 mice (Walter and Eliza Hall Institute) or in-house NOD-Prkdc^{scid}IL2rg^{null} (NSG) male mice (6–8 weeks old) were inoculated subcutaneously with 2 million cells in phosphate-buffered saline (PBS). Male mice were used as the Yumm1.7 was a male-derived cell line.[25] Tumor volumes were calculated as 0.5×length×(width)^2. Once tumors reached an average size of 100–200 mm^3, mice were randomized into treatment groups to ensure an even distribution of tumor sizes. As an ethical endpoint, mice were euthanized when the tumors exceeded 1,200 mm^3. TT were administered orally (dabrafenib: 30 mg/kg, trametinib: 0.3 mg/kg, erlotinib: 100 mg/kg, napabucasin: 100 mg/kg) via daily gavage in 0.5% hydroxypropyl-methyl cellulose, 0.2% Tween-80 in H_2O (6–7 days/week). AC-4–130 (12.5 mg/kg) was delivered intraperitoneally for 21 days in 10% DMSO, 5% Kolliphor EL (BASF, Cat.no. 30554032) diluted in saline. Anti-PD-1 (Bio X Cell, RMP1-14, Cat.no. BE0146) and anti-CTLA-4 (9H10, Cat.no. BE0131) were given intraperitoneally as combinations (initial: 200/150 µg; subsequent: 150/100 µg) 4 days apart. Anti-CD8β (53–5.8, Cat. no. BE0223) was administered every 3 days intraperitoneally (initial: 200 µg; subsequent: 100 µg). Drugs were prepared fresh daily, except erlotinib (stored at 4°C weekly). For tumor immune microenvironment analysis, TT were administered 3 hours prior to tumor harvest.

Tumor preparation and flow cytometry

Tumors were processed as mentioned above, and the solution was washed and stained with LIVE/DEAD Fixable Dye, followed by a conjugated antibody cocktail. After washing, cells were fixed and stained intracellularly. Antibodies used included BD Biosciences: CD45.2 (104), TCRbeta (H57-597), CD44 (IM7), Tim3 (5D12), Ly6G (1A8), Ly6C (AL-21), PD-L1 (MIH5); BioLegend: CD8 (53–6.7), CD4 (RM4-5), CD62L (mel-14), PD-1 (29F.1A12), CD11b (M1/70), CD11c (N418), F4/80 (BM8), CD163 (S15049F), H2Db (34-5-8S), H2Kb (AF6-88.5), PD-L1 (10F.9G2); Thermo Fisher: FOXP3 (FJK-16s), CD86 (GL1), CD80 (16–10 A1), MHC-II (M5/114.15.2). Stained cells were analyzed on a BD FACSymphony flow cytometer and data processed with FlowJo (V.10). For t-distributed Stochastic Neighbor Embedding (t-SNE) analysis in online supplemental figure S2B, equal numbers of live CD45.2+cells from each sample were concatenated and processed using FlowJo's t-SNE function for dimensionality reduction with all antibody markers. Samples were then grouped based on pre-assigned labels to identify distinct populations within each treatment arm.

Dose response assays

Cells were plated in pentaplicate in a 96-well plate at 600 cells/well and incubated for 24 hours. Treatments with vehicle (DMSO) or escalating drug doses were applied, and a T0 plate was set-up for data normalization. The T0 plate was fixed with methanol for 5 min, then stored at 4°C. After 3 days of treatment, all plates were fixed with methanol, treated with 100 µL/well of 2N HCL+0.5% Triton X-100 for 20–30 min, followed by Sodium tetraborate decahydrate ($Na_2B_4O_7$. $10H_2O$) for 10 min, and stained with propidium iodide (PI) (1mg/1ml) at 1 in 1000 dilution for nuclei visualization. Cell numbers were measured using IncuCyte (Essen-BioScience), normalized to T0 values, and plotted against drug concentrations.

Proliferation assays

Cells were seeded at 100–200 cells/well in a 96-well plate and allowed to adhere overnight. After treatment with pharmacological inhibitors, cell confluency was recorded every 12 hours using IncuCyte. TT were added with six technical replicates per group, followed by incubation under standard conditions. Confluency was calculated as a percentage of well area using the IncuCyte's boundary recognition algorithm.

Western blot analysis

After treatment with pharmacological inhibitors, cells were rinsed with PBS and lysed using western solubilization buffer (0.5 mM EDTA, 20 mM HEPES, pH 7.9, 2% Sodium Dodecyl Sulfate (SDS)). Lysates were homogenized and denatured at 95°C for 5 min. Protein concentration was quantified using a DC protein assay (Bio-Rad, cat no. 5000111) and measured at 750 nm on a Benchmark microplate reader (Bio-Rad). Samples were diluted in 5× SDS sample buffer (313 mM Tris·HCl, pH 6.8, 50% glycerol, 10% β-mercaptoethanol, 10% SDS, 0.05% bromophenol blue) and separated on TGX stain-free gels (Bio-Rad). A Precision-plus protein dual-color standard (Bio-Rad, cat no. 1610374) was used for molecular weight determination. Proteins were transferred

to polyvinylidene fluoride (PVDF) membranes (Millipore) using a semi-dry transfer system. Membranes were blocked for 1 hour in 5% skim milk in TBS-T, then incubated overnight with primary antibodies (p-ERK (1:1000, Cat.no. 4370S), T-ERK (1:1000, Cat.no. 9102L), STAT3 (1:500, Cat.no. 9139T), STAT5 (1:500, Cat.no. 94205T)) or for two nights with EGFR (1:200, E0913, Santa Cruz), p-STAT3 (1:200, Cat.no. 9131), and p-STAT5 (1:200, Cat.no. 9351). After incubation, Horseradish Peroxidase (HRP) -conjugated secondary antibodies were applied for 1 hour at room temperature. Blots were washed in TBS-T and visualized using chemiluminescence (Bio-Rad, Cat. no. 1705061) on the ChemiDoc Imaging System (Bio-Rad). Tubulin was used as the loading control. Antibodies were sourced from Cell Signaling Technology (STAT3, STAT5, p-ERK, T-ERK, p-STAT3, p-STAT5) and Santa Cruz (EGFR, NRAS).

Immunohistochemistry

Tumors were harvested, weighed, and fixed in 10% neutral buffered formalin overnight before paraffin embedding. Sections (4 µm) were cut and processed using the Jung XL Autostainer (Leica) for dewaxing and rehydration, followed by antigen retrieval in 10 mmol/L citrate buffer (Agilent, Cat.no. S2367, pH 9) at 125°C for 3 min. After washing with MiliQ water and wash buffer (1× TBS+0.05% Tween-20), slides were blocked with 3% H_2O_2 for 10 min. After another wash, slides were incubated with primary antibodies (BrdU (1:200, BD Bioscience, Cat.no. 347580), p-ERK (1:200, Cell Signaling Technology, Cat. no. 4370S)) for 1 hour at room temperature, followed by incubation with Dako secondary antibody (Agilent, Cat.no. K4003) for 1 hour. DAB chromogen staining was performed for 5–10 min, followed by rinsing with distilled water. Hematoxylin counterstaining was done using the Jung XL Autostainer. Slides were mounted with coverslips, and images were captured using a VS200 confocal microscope (Olympus). Slide analysis and quantification were performed using HALO or QuPath software.

Viral transfection and transduction

A retroviral-mediated system was used to construct $NRAS^{G12D}$ or control empty vector (EV) YR1.7PV1 cells. The empty and $NRAS^{G12D}$ (pMSCV-NRASG12D-IRES-mCherry) plasmids were gifted by Dr Stefan Bjelosevic from PeterMac. HEK293T cells were transfected with 3.5 µg of pEQ and RD114 packaging plasmids and 14 µg of gene-specific plasmid per T175 flask, alongside 42 µL Fugene HD (1:3 ratio with reporter DNA, Promega, cat. no. E2311) in non-supplemented DMEM. Fresh media was added after 24 hours, and viral supernatants were collected every 8–10 hours for 3 days, filtered (0.45 µm), and concentrated using Amicon Ultra-15 Centrifugal Filter (Millipore, cat. no. UFC9100). The virus was stored at −80°C and added to target cells at a 1:30 ratio with 1 µg/mL polybrene. After 72 hours, cells were expanded and selected for $mCherry^{mid}$ expression by fluorescence-activated cell sorting.

RNA isolation

RNA was isolated using the NucleoSpin RNA extraction kit from Macherey Nagel (740955.250) according to the provided manufacturing instructions.

RNA sequencing and data analysis

RNA quality was assessed using Agilent RNA TapeStation (Agilent Technologies), with samples having RNA integrity number >9 submitted for sequencing. 1 µg of RNA was used for 3' RNA library preparation following manufacturer's instructions (QuantaSeq, Lexogen). Sequencing and library preparation were conducted by the Molecular Genomics Core at Peter MacCallum Cancer Centre, Australia.

Reads were aligned and processed using Galaxy. FastQ files were loaded, and Illumina adaptors were trimmed using Cutadapt (V.3.7). Sequences were aligned to the mm10 mouse genome using HISAT2 (V.2.2.1), generating raw counts matrices. Differentially expressed genes (DEGs) were identified using limma-voom, applying a >0.5 counts per million threshold in more than three samples.[26] For patient data set (GSE65185), the transcripts per million were generated from fragments per kilobase millions by normalizing the counts and then scaling them to a per million bases. Gene Set Enrichment Analysis (GSEA) was performed on pre-ranked DEGs using ClusterProfiler and run against the C6:Oncogenic and H:Hallmarks gene sets.[27 28] Gene Set Variation Analysis (GSVA)[29] analysis was conducted on normalized counts generated from the voom object, and was run against hallmarks and C6 gene sets, using and normalizing against single sample GSEA. In order to obtain the immune score, the immunedeconv package[30] was used to run the ESTIMATE algorithm.[31]

Statistical analysis

Results obtained are presented as mean±SEM unless otherwise stated. Unpaired Student's t-test or one-way analysis of variance was used to compare two or more independent groups, respectively. Survival curves were compared using the log-rank (Mantel-Cox) test. P values: *p<0.05, **p<0.01, ***p<0.001, ****p<0.0001. n=number of biological replicates.

DATA AVAILABILITY

RNA sequencing (RNAseq) data from this study is available as an online supplemental file. The patient data set is available under gene expression omnibus (GEO) accession code GSE65185.[15]

RESULTS

Development of melanoma model with acquired resistance to BRAF/MEK inhibition

The Yummer (YR) 1.7 cell line was initially used because of its immunogenicity and sensitivity to both TT and ICI.[24 32] However, this line had an inherent susceptibility

to rejection when injected into C57BL/6 mice (online supplemental figure S1A). To circumvent this issue, a YR1.7 tumor that had escaped host control was collected and processed for long-term culture ex vivo (online supplemental figure S1A). This YR1.7 passage variant (YR1.7PV1) successfully grew in C57BL/6 mice (online supplemental figure S1B) despite evoking host immune activity (online supplemental figure S1C). *In vitro*, these cells maintained sensitivity to BRAFi/MEKi (online supplemental figure S1D) and *in vivo* were responsive to BRAFi/MEKi (online supplemental figure S1E) and anti-CTLA-4/anti-PD-1 (online supplemental figure S1F) treatment.

To model acquired resistance (AR), the YR1.7PV1 cell line was progressively exposed to increasing concentrations of BRAFi/MEKi *in vitro* for 6 months. *In vitro*, dose-response and proliferation assays confirmed reduced responsiveness to BRAFi/MEKi in AR cells compared with the Parental YR1.7PV1 cells, with higher growth inhibition (GI) 50% value and continued proliferation at the GI90 dose effective against Parental cells (figure 1A,B). Since increased MAPK/ERK activity commonly underlies resistance to BRAFi/MEKi treatment,[16 17] we examined whether this pathway was overactivated in the AR cells. BRAFi/MEKi treatment decreased pERK levels in both YR1.7PV1 Parental and AR cells (figure 1C), suggesting that drug resistance in AR cells is independent of the MAPK/ERK pathway.

YR1.7PV1 AR cells are sensitive to CD8+ T-cell mediated immune control

In immunodeficient NSG mice, the YR1.7PV1 AR tumors grew at a comparable rate to that observed for the Parental cell line (figure 1D). However, as expected, only the YR1.7PV1 tumors were responsive to BRAFi/MEKi treatment, with a significant decrease in tumor growth and increased survival time (figure 1D). Failure of the YR1.7PV1 AR tumors to respond to BRAFi/MEKi in NSG mice confirmed maintenance of the drug-resistant phenotype *in vivo*. We then evaluated sensitivity to BRAFi/MEKi in immune-competent C57BL/6 mice. Interestingly, AR tumors demonstrated partial responsiveness to BRAFi/MEKi, resulting in a survival response similar to Parental counterparts (figure 1E). This suggests that BRAFi/MEKi treatment enhances AR tumor immunogenicity, increasing sensitivity to immune control. Immunohistochemical analysis of the tumors from the control and BRAFi/MEKi treated C57BL/6 mice confirmed that only the YR1.7PV1 Parental tumors were sensitive to the antiproliferative effects of BRAFi/MEKi treatment, evident by the significant loss of BrdU staining compared with the AR tumors (figure 1F). Notably, loss of pERK expression following BRAFi/MEKi treatment was evident in both tumor groups, supporting our conclusion that the establishment of resistance in the YR1.7PV1 AR cell line was independent of the MAPK/ERK pathway (figure 1G).

To further examine the immune system's role in the treatment response of AR cells in C57BL/6 mice, we used flow cytometry to analyze the immune microenvironment of YR1.7PV1 parental and AR tumors on days 5 and 15 post-BRAFi/MEKi treatment initiation (figure 2A). At day 5 (figure 2B,C), a significant infiltration of CD8+effector T cells (Teff, $CD44^{+}CD62L^{low}$) was detected in the YR1.7PV1 AR tumors, which was not significantly evident in the treated Parental counterpart. Notably in YR1.7PV1 AR tumor settings, BRAFi/MEKi treatment reduced the frequency of tumor-associated Teff CD8+T cells with an exhaustion phenotype ($PD\text{-}1^{+}TIM3^{+}$; figure 2C). Interestingly, although the YR1.7PV1 AR tumors exhibited an elevated CD8+T effector cell response, this was accompanied by only a modest increase in $FOXP3^{+}$ T regulatory cells (Tregs), resulting in no significant change in the Treg:CD8+T cell ratio. In contrast, BRAFi/MEKi treatment led to an increased CD4+T cell response in the Parental tumors, which was associated with a higher Tregs and hence Treg:CD8+T cell ratio (figure 2C). These trends in tumor-immune composition in the YR1.7PV1 Parental and AR tumors persisted out to day 15 of BRAFi/MEKi treatment (figure 2D,E). Meanwhile, no significant differences in tumor-associated myeloid cells were identified between the YR1.7PV1 Parental and AR tumors at days 5 (figure 2F and online supplemental figure S2A–C) and 15 (figure 2G) of treatment. In both tumor settings, BRAFi/MEKi treatment was observed to induce an increased frequency of $CD103^{+}$ cross-presenting dendritic cells and a marked decrease in polymorphonuclear myeloid-derived suppressor cells (PMN-MDSCs) (figure 2F). Examining the expression of MHC-I, PD-L1 and CD80 revealed an induction of H2-Kb in the YR1.7PV1 AR tumor cells at day 5, a trend that did not persist out to day 15 of treatment (online supplemental figure S2D,E). Loss of PD-L1 expression was only significant in the AR tumor cells at day 5 of BRAFi/MEKi treatment compared with vehicle control; however, by day 15, its expression was elevated in AR tumor cells relative to Parental (online supplemental figure S2D,E). Interestingly, CD80 expression was significantly lower in the YR1.7PV1 AR tumor cells compared with Parental tumor cells (online supplemental figure S2D). While BRAFi/MEKi-mediated reduction of CD80 expression was observed in the Parental tumors (online supplemental figure S2D) no drug-induced change was detected in the AR tumors (online supplemental figure S2D,E). Together, these data suggest that the YR1.7PV1 AR tumors have a heightened sensitivity to the immune modulatory effects of BRAFi/MEKi treatment, compared with YR1.7PV1 Parental tumors.

To evaluate the role of CD8+T cells in the antitumor activity of BRAFi/MEKi in AR tumors, C57BL/6 mice were treated with anti-CD8 depleting antibodies during the first 12 days of treatment (figure 2H). Loss of CD8+T cells resulted in AR tumors escaping more rapidly on treatment. A significant reduction in overall survival was also observed relative to the immune competent control mice (figure 2H). These data further highlight the immune modulatory effects of BRAFi/MEKi treatment, which can be induced independently of the drugs' direct impact on tumor cell proliferation.

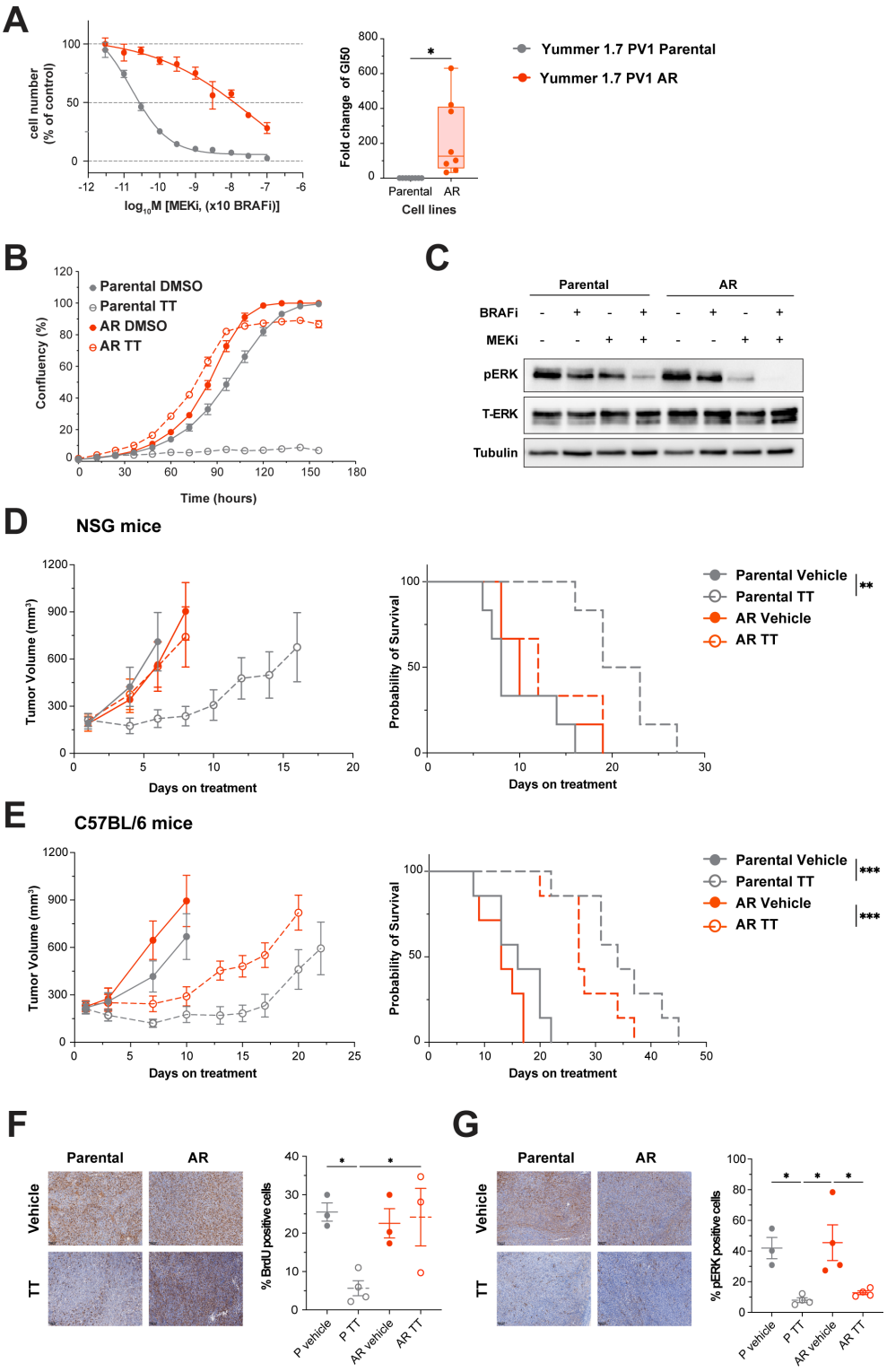

Figure 1 YUMMER 1.7PV1 AR cells are resistant to BRAFi/MEKi in an immune-compromised setting but not in an immune-competent setting. (A) 3-day dose response assay of Parental and acquired resistant (AR) cell lines, and their fold change in the dose of drug required to inhibit growth by 50% (GI50). For the bar graph, error bars show mean±SEM from eight independent experiments. (B) Proliferation of Parental and AR cells treated with 100/10 nM of BRAFi/MEKi. Representative of at least three independent experiments. Error bars show mean±SEM of 6 technical replicates. (C) Western blot on protein lysates after 3 days of treatment with 100 nM of BRAFi 10 nM of MEKi or their combination. A representative of two independent experiments. (D) YUMMER 1.7PV1 Parental and AR tumor volumes and survival curves in NSG mice (n=6 mice for each group) and (E) in C56BL6 mice (n=7 mice for each group). (F) BrdU IHC analysis of tumors from C57BL/6 treated with BRAFi/MEKi for 5 days (G) IHC analysis of pERK. Scale bar—100 µm. Log-rank (Mantel-Cox) test used for two survival curve comparison. For group comparisons, one-way analysis of variance test is used. *p<0.05; **p<0.01; ***p<0.001. AR, acquired resistance; BRAFi/MEKi, BRAF/MEK inhibitors; TT, targeted therapy - combination of BRAFi (dabrafenib) and MEKi (trametinib).

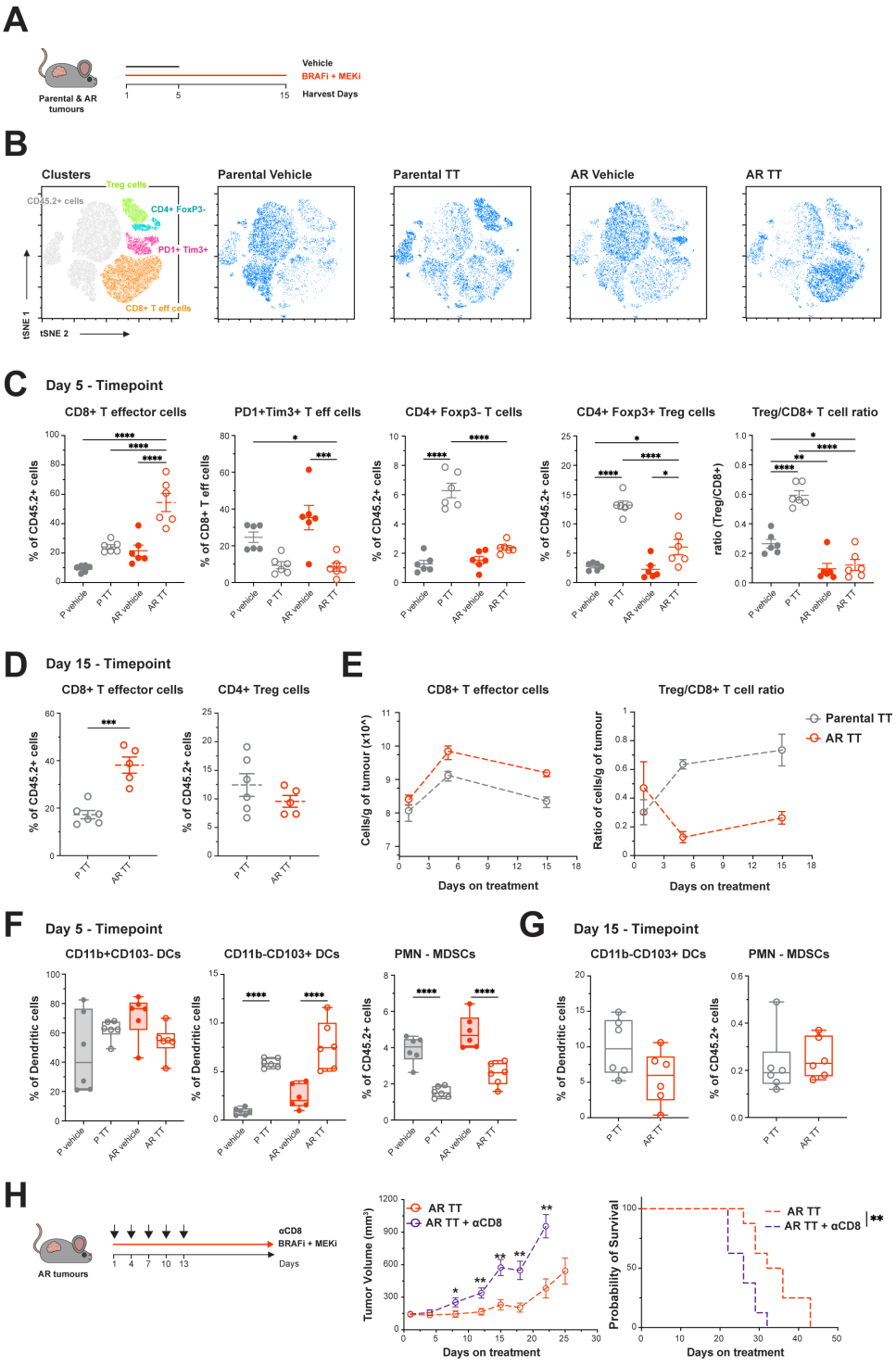

Figure 2 CD8+T effector cells are upregulated in YUMMER 1.7PV1 AR-treated tumors. (A) Schematic of the harvest time points whereby four groups (AR and Parental±treatment) were harvested at day 5 and two groups at day 15 (AR and Parental, treated only). (B) and (C) CD45.2+cells from Parental and AR tumors analyzed by flow cytometry at day 5 of treatment. One-way ANOVA multiple tests, n=6. Mean±SEM. (D) CD45.2+cells from TT-treated Parental and AR tumors analyzed by flow cytometry at day 15. Unpaired Student's t-test, n=6. Mean±SEM. (E) Total number of CD8+T effector cells and the ratio of Treg cells to CD8+T cells are plotted against time. N=6 per group, per time point. Mean±SEM. (F) Box plot analysis of tumor-associated myeloid populations of Parental and AR tumors analyzed by flow cytometry at day 5 and (G) day 15. One-way ANOVA test or unpaired Student's t-test done for comparison, respectively. n=6 per group, per time point. Mean±minimum/maximum value. (H) Tumor volume and survival curves of AR cells with BRAFi/MEKi±CD8 depletion. Mean±SEM. n=8 mice per group. Unpaired Student's test performed to compare tumor sizes and log-rank (Mantel-Cox) test used for two survival curve comparisons. *p<0.05; **p<0.01; ***p<0.001; ****p<0.0001. ANOVA, analysis of variance; AR, acquired resistance; BRAFi/MEKi, BRAF/MEK inhibitors; PMN-MDSCs, polymorphonuclear myeloid-derived suppressor cells; TT, targeted therapy, combination of BRAFi (dabrafenib) and MEKi (trametinib); Treg, regulatory cells.

YR1.7PV1 AR tumors respond to ICI treatment following BRAFi/MEKi therapy

Building on our findings that YR1.7PV1 AR tumors elicit an immune response following treatment with BRAFi/MEKi, we investigated their vulnerability to anti-PD-1/anti-CTLA-4 ICI relative to Parental tumors. In both settings, ICI significantly delayed tumor growth and prolonged survival in a similar manner (figure 3A). Simultaneous treatment with ICI and BRAFi/MEKi for 12 days significantly delayed tumor growth and prolonged survival, relative to the single modality treatments in both the YR1.7PV1 Parental and AR tumors (figure 3B). However, a 50% cure rate was only achieved in mice bearing the Parental tumors, whereas all mice with AR tumors eventually succumbed to disease (figure 3B). These data suggest additional mechanisms of BRAFi/MEKi-mediated disease control in the YR1.7PV1 tumors, which are absent in the AR tumors.

Building on the observed capacity of BRAFi/MEKi treatment to induce a significant increase in CD8+T effector cells within the YR1.7PV1 AR tumors (figure 2), we hypothesized that treatment of the AR tumors with BRAFi/MEKi for 5 days would enhance their response to second-line ICI. Sequential administration of ICI significantly delayed tumor growth and prolonged survival in mice bearing Parental and AR tumors (figure 3C). However, over 50% of the mice bearing AR tumors survived longer than those with Parental tumors. Taken together, these data highlight that YR1.7PV1 AR tumors are less prone to the development of cross-resistance to ICI compared with the YR1.7PV1 tumors.

The EGFR-STAT pathway is upregulated in YR1.7PV1 AR tumor cells

To elucidate the BRAFi/MEKi-resistance mechanism supporting heightened immunological responses *in vivo*, we conducted transcriptomic analysis on the YR1.7PV1 Parental and AR cell lines after *in vitro* BRAFi/MEKi treatment (figure 4A). Multidimensional scaling of RNA-seq data revealed a distinct separation between AR and Parental cells, with treatment further amplifying differences in gene expression (figure 4B). Differential gene expression analysis between untreated Parental and AR cells identified 1,437 significantly upregulated genes including *EGFR*, *STAT5a*, and *STAT3* (figure 4C). GSEA revealed an upregulation of immune-related pathways such as interferon (IFN)-alpha and IFN-gamma as well as interleukin (IL)-2-STAT5, IL-6-STAT3 and EGFR signaling in untreated YR1.7PV1 AR cells compared with untreated Parental cells (figure 4D,E). Due to the one-way comparison limitation of GSEA, we employed GSVA to compare a combination of hallmark and C6 gene sets that were found to be significantly upregulated in YR1.7PV1 AR cells. Notably, this analysis further provided evidence of increased activity in IL-6-STAT3, IL-2-STAT5, and EGFR signaling pathways in AR cells, with these pathways being more highly expressed with BRAFi/MEKi treatment (figure 4F). These findings suggest that these pathways may play an important role in the survival of AR cells under BRAFi/MEKi treatment.

To validate these RNA-seq findings, we assessed the expression levels of EGFR and STAT proteins. EGFR messenger RNA (figure 4G) and protein (figure 4H) were significantly upregulated in the YR1.7PV1 AR cells compared with Parental cells, with EGFR protein expression further increasing in AR cells with BRAFi/MEKi treatment. Additionally, AR cells showed an increased expression of both STAT3 and STAT5. Notably, both of these proteins were found to be phosphorylated in BRAFi/MEKi treated YR1.7PV1 AR cells but not in Parental cells (figure 4H). These results are consistent with upregulation of EGFR or STAT signaling pathways driving proliferation of AR cells following treatment with BRAFi/MEKi.

STAT proteins can be phosphorylated by either EGFR or Janus kinase (JAK),[33 34] we therefore hypothesized that co-treatment with erlotinib (EGFRi) or ruxolitinib (JAKi), in combination with dabrafenib (BRAFi) and trametinib (MEKi), would reduce AR cell proliferation *in vitro*. The combination of EGFRi with BRAFi/MEKi resulted in a significant reduction in YR1.7PV1 AR cell proliferation compared with BRAFi/MEKi alone (figure 5A). This was not observed when AR cells were treated with a JAKi plus BRAFi/MEKi (online supplemental figure S3B), suggesting that proliferation of AR cells following treatment with BRAFi/MEKi is predominantly driven by EGFR signaling rather than JAK signaling.

To explore the involvement of the EGFR-STAT pathway in the proliferative activity of YR1.7PV1 AR cells, we hypothesized that inhibiting EGFR would reduce STAT protein phosphorylation. Indeed, BRAFi/MEKi-induced phosphorylation of both STAT3 and STAT5 was reduced with the addition of an EGFRi, suggesting EGFR-mediated phosphorylation of these proteins (figure 5B). Moreover, when BRAFi/MEKi and EGFRi were combined with either a STAT3i (napabucasin: figure 5C) or STAT5i (AC-4–130: figure 5D), there were additive effects on the inhibition of AR cell proliferation. Western blot analysis for the different drug combinations revealed a reduction in pSTAT3 and pSTAT5 levels with the combination of BRAFi/MEKi plus EGFRi plus their respective inhibitors (figure 5E,F).

To further examine these observations *in vivo*, C57BL/6 mice bearing YR1.7PV1 AR tumors were treated with BRAFi/MEKi+EGFRi for 21 days. The BRAFi/MEKi and EGFRi combination significantly delayed tumor growth and prolonged survival compared with mice treated with either treatment alone (figure 5G). Notably, the administration of an STAT3i or STAT5i could also prolong the effects of BRAFi/MEKi treatment in C57BL/6 mice bearing YR1.7PV1 AR tumors (online supplemental figure S3C,D). However, the combination of BRAFi/MEKi/EGFRi and STAT3i or STAT5i achieved no additional therapeutic benefit (online supplemental figure S3C,D), suggesting EGFR and STAT3/5 may act on the same pathway. These findings are consistent with the

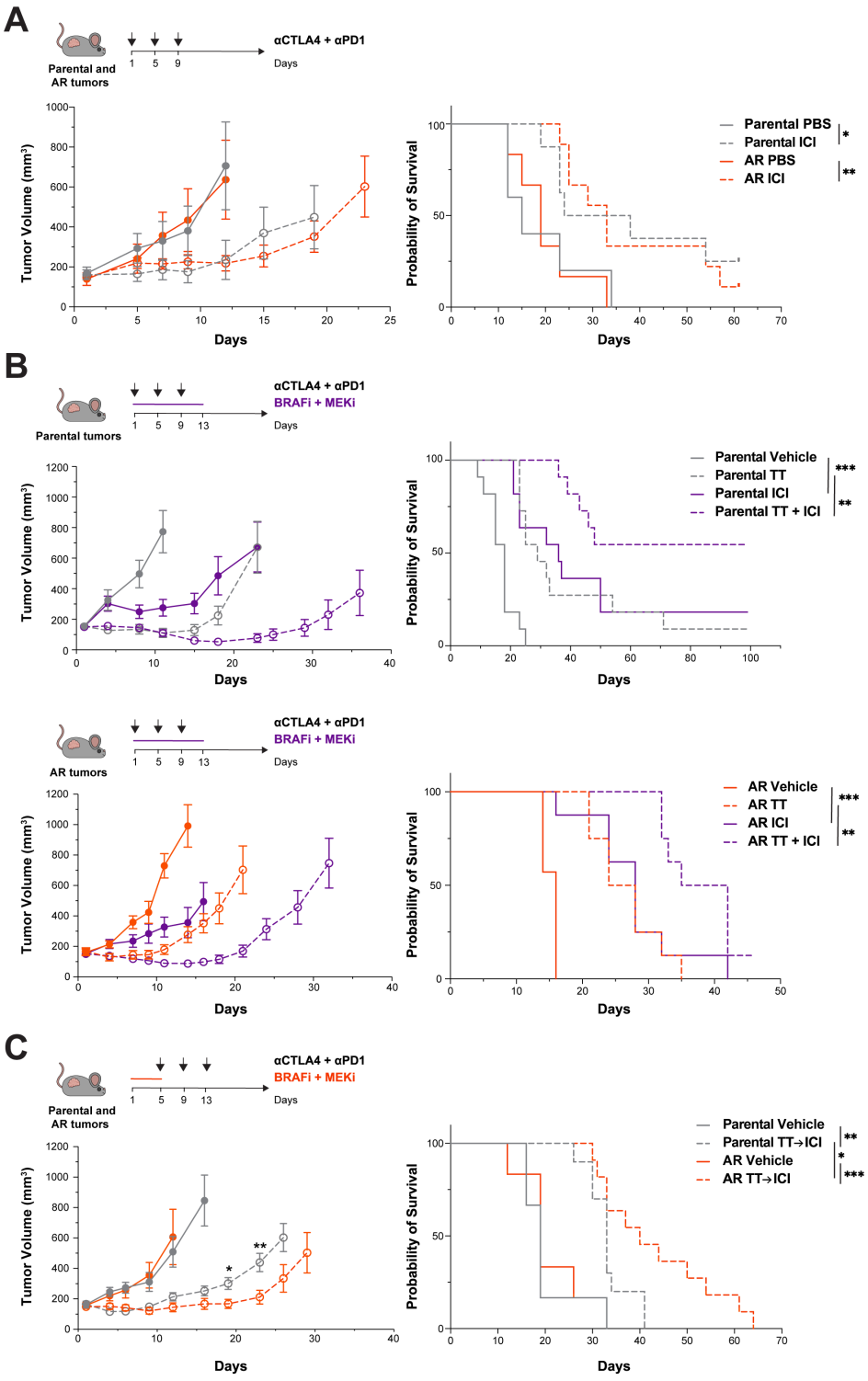

Figure 3 Upfront and sequential BRAFi/MEKi and immune checkpoint inhibitors in YUMMER1.7PV1 Parental and AR tumors. Tumor volume and survival curves for both YUMMER 1.7PV1 Parental and AR tumors in C57BL/6 mice. Each figure shows the treatment schedule with arrows indicating intraperitoneal injection of ICI and the lines indicating daily treatment with BRAFi/MEKi. (A) Mice were treated with three doses of ICI, 4 days apart. Parental PBS—n=5, Parental ICI—n=8, AR PBS n=6 and AR ICI n=9 mice per group. (B) Parental tumor (Top, n=11 mice per group) and AR tumor (bottom, n=8 mice per group) bearing mice were treated with the combination of TT for 12 days and 3 doses of ICI, 4 days apart. (C) AR and Parental tumor-bearing mice were treated with 5 days of TT followed by three doses of ICI, 4 days apart. Parental Vehicle n=6, Parental TT→ICI n=10, AR Vehicle n=6, AR TT→ ICI n=11 mice per group. Mean±SEM shown. Unpaired Student's t-test performed to compare tumor sizes and log-rank (Mantel-Cox) test used for two survival curve comparison. *p<0.05; **p<0.01; ***p<0.001, ****p<0.0001. AR, acquired resistance; BRAFi/MEKi, BRAF/MEK inhibitors; CTLA-4, cytotoxic T lymphocyte antigen-4; ICI, immune checkpoint inhibitor; PBS, phosphate-buffered saline; PD-1, programmed cell death-1; TT, targeted therapy, combination of BRAFi (dabrafenib) and MEKi (trametinib).

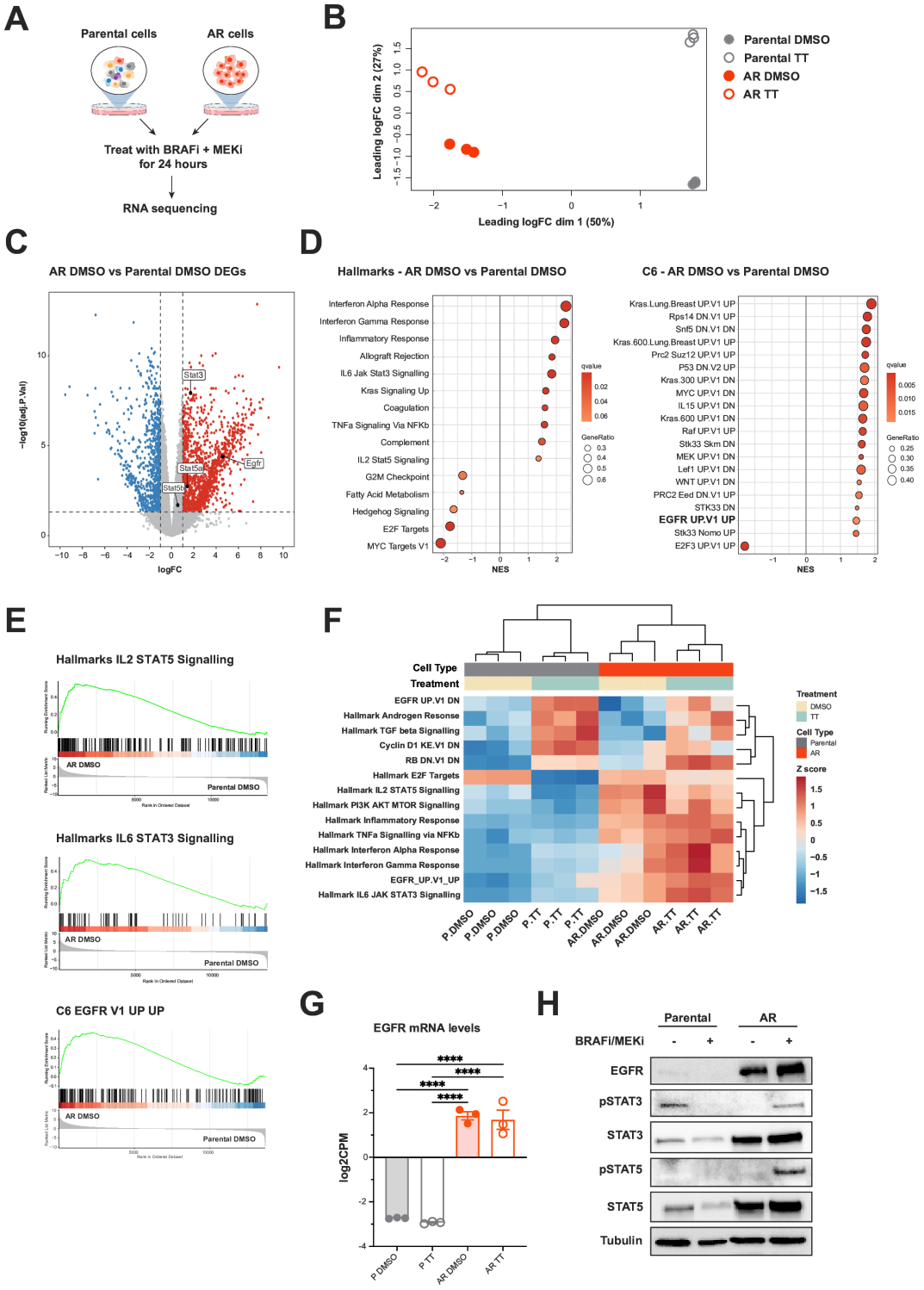

Figure 4 RNA sequencing of YUMMER 1.7PV1 AR cells reveals upregulation of the EGFR-STAT pathway. (A) Schematic of treatment for RNA sequencing. Both Parental and AR cells were treated with the combination of BRAFi/MEKi at 100/10 nM for 24 hours in vitro. (B) Multidimensional scaling highlighting gene expression differences between samples. Each dot represents one sample, with n=3 per group. (C) Volcano plot of differentially-expressed genes (DEGs) in AR cells versus Parental untreated cells. (D) Gene Set Enrichment Analysis comparing untreated Parental and AR cells, using the H: Hallmarks gene sets and C6: Oncogenic signature gene set. (E) EGFR gene set, and STAT signaling gene set enrichment plots that were found to be significantly upregulated in AR versus Parental untreated cells. (F) Gene Set Variation Analysis scores across samples of AR and Parental cells±treatment. (G) EGFR mRNA expression from the RNA sequencing data. n=3 per group. Mean±SEM. One-way analysis of variance test. (H) Western blot on protein lysates after 3 days of treatment with the combination of 100 nM of BRAFi and 10 nM of MEKi in vitro. A representative of two independent experiments. ****p<0.0001. AR, acquired resistance; BRAFi/MEKi, BRAF/MEK inhibitors; IL, interleukin; mRNA, messenger RNA; TT, targeted therapy, combination of BRAFi (dabrafenib) and MEKi (trametinib).

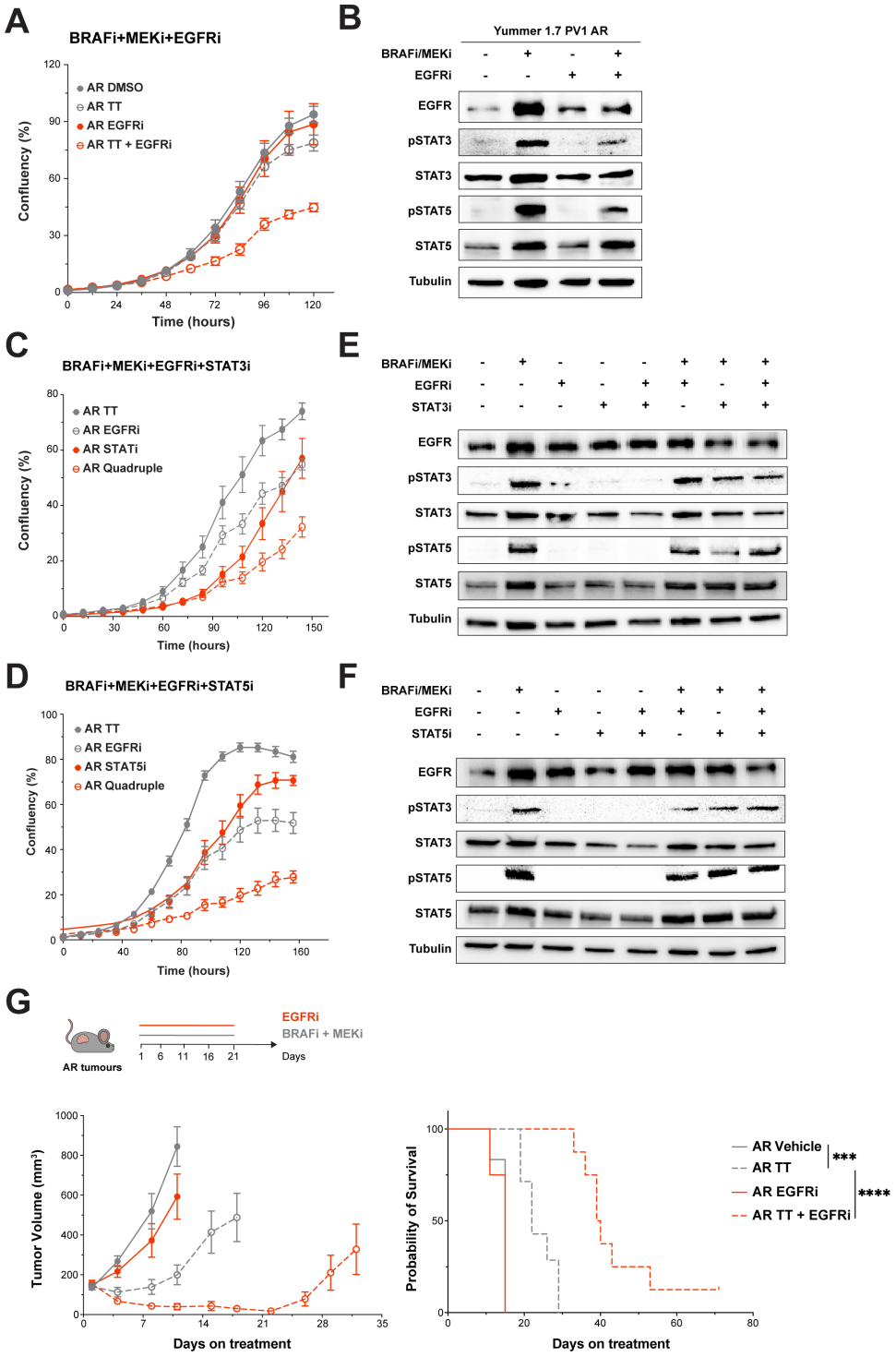

Figure 5 EGFR inhibition restores sensitivity in YUMMER 1.7PV1 AR cells to BRAFi/MEKi. (A) In vitro proliferation assay of AR cells treated with 100/10 nM of BRAFi/MEKi in combination with 2 µM of EGFRi. Representative of at least three independent experiments, error bars show Mean±SEM of 6 technical replicates. (B) Western blot on protein lysates from cells treated for 3 days with the combination of 100/10 nM of BRAFi/MEKi and 2 µM of EGFRi. A representative of two independent experiments. In vitro proliferation assay of AR cells treated with various combinations of 100/10 nM of BRAFi/MEKi, 2 µM of EGFRi, 200 nM of STAT3i (C) and 1 µM of STAT5i (D). Representative of at least three independent experiments, error bars show Mean±SEM of 6 technical replicates. (E–F) Western blot on protein lysates from cells treated for 3 days with the various combinations of 100/10 nM of BRAFi/MEKi, 2 µM of EGFRi, 1 µM of STAT5i and 200 nM of STAT3i. A representative of two independent experiments. (G) Tumor volume and survival curves of AR tumors treated with the combination of BRAFi/MEKi and EGFRi in C57BL/6 mice. The mice were treated for 21 days and then the treatment was stopped. Mean±SEM. Vehicle—n=7, BRAFi/MEKi—n=7, EGFRi—n=8, BRAFi/MEKi+EGFRi—n=8 mice per group. Log-rank (Mantel-Cox) test is used for survival comparison. ***p<0.001, ****p<0.0001. TT, targeted therapy, combination of BRAFi (dabrafenib) and MEKi (trametinib), erlotinib (EGFRi), napabucasin (STAT3i) and AC-4–130 (STAT5i). AR, acquired resistance; BRAFi/MEKi, BRAF/MEK inhibitors.

theory that *in vitro* and *in vivo* proliferation of YR1.7PV1 AR cells under BRAFi/MEKi treatment is driven by the EGFR-STAT pathway.

NRAS^{G12D}-driven BRAFi/MEKi-resistance confers cross-resistance to ICI

To evaluate the impact of alternative resistance mechanisms on ICI sensitivity, we investigated NRAS^{G12D}-driven MAPK/ERK reactivation, a common clinical event.[35 36] We engineered an NRAS^{G12D} mutant YR1.7PV1 cell line which *in vitro* demonstrated reduced sensitivity to BRAFi/MEKi (figure 6A), sustained proliferation under treatment (figure 6B), and elevated pERK levels that were only partially inhibited by BRAFi/MEKi, comparable to untreated controls (figure 6C). In C57BL/6 mice, NRAS mutant YR1.7PV1 tumors grew more aggressively compared with control tumors and were resistant to the antitumor effects of BRAFi/MEKi treatment, showing no evident change in tumor growth or survival (figure 6D). Immunohistochemical analysis revealed persistently elevated pERK levels despite treatment in NRAS mutant tumors, suggesting that the NRAS^{G12D} mutation drives resistance to BRAFi/MEKi therapy by reactivation of MAPK/ERK signaling (figure 6E). Notably, these NRAS mutant tumors were also resistant to ICI, indicating that the NRAS^{G12D} mutation and associated activation of the MAPK/ERK pathway may dampen the immunogenicity of tumor cells or evoke an immunosuppressive tumor microenvironment (figure 6F). Collectively, these findings demonstrate that NRAS^{G12D}-driven MAPK/ERK upregulation promotes resistance to both BRAFi/MEKi and ICI, whereas EGFR upregulation, despite inducing BRAFi/MEKi resistance, may enhance ICI responsiveness.

Elevated EGFR correlates with an ICI-responsive immune score in patients with melanoma

To further explore the complex relationship between EGFR signaling and sensitivity to second-line ICI in patients, we analyzed previously published RNA-seq data.[15] This data set includes matched pretreatment and post-progression melanoma biopsies from individuals who received BRAFi±MEKi treatment. Using the GSVA algorithm to analyze the gene sets upregulated in BRAFi/MEKi-treated YR1.7PV1 AR cells, patients were found to have varying levels of expression for the "EGFR UP V1 UP" signature. Many showed higher expression, suggesting that EGFR-driven pathways may contribute to resistance in a subset of these patients (figure 7A). Consistent with findings from the YR1.7PV1 AR tumor model (figure 4F), unsupervised clustering showed that the EGFR gene signature clustered with IL-6-STAT3, IL-2-STAT5 and tumor necrosis factor-alpha (TNF-a) signatures, suggesting a potential association (figure 7A). Furthermore, stratifying patients with melanoma with high (Z score >0), or low (Z score <0) "EGFR UP V1 UP" gene signature revealed that patients with elevated EGFR signatures had a high immune score as determined by the ESTIMATE algorithm (figure 7B,C). These clinical data suggest enhanced immune infiltration is associated with an EGFR signature in melanoma, raising the possibility that this signature could be a biomarker of response to ICI. Consistent with this possibility, we observed a strong positive correlation between pretreatment and post-progression immune scores, indicating that patients with an EGFR signature and higher immune scores pretreatment tend to maintain higher immune scores post-progression (figure 7C). To determine if this correlation was specific to the EGFR signature, we analyzed the EGFR scores pretreatment and post-treatment for each patient. Surprisingly, patients with a higher EGFR signature before treatment also tended to have a higher EGFR signature after treatment (figure 7D), which interestingly correlated with the immune score (figure 7E, online supplemental table S1). These data highlight a potential link between EGFR signature upregulation and heightened immune infiltration, potentially shaping the response to second-line ICI in patients with melanoma progressing on first-line BRAFi/MEKi. These findings align with our YR1.7PV1 AR model, which shows a similar immune infiltration pattern that is associated with EGFR signaling and sensitivity to ICI.

DISCUSSION

Clinical studies show that cross-resistance to second-line ICI is common after BRAFi/MEKi-resistance develops, though some patients remain responsive. Understanding the mechanisms of BRAFi/MEKi resistance and its impact on the tumor microenvironment is key to identifying patients likely to benefit from second-line ICI therapy. In this study, we demonstrate that BRAFi/MEKi-resistant tumors, driven by upregulation of the EGFR-STAT pathway, maintain sensitivity to second-line ICI therapy. In this context, BRAFi/MEKi fosters an immune-activating microenvironment in the AR tumors, characterized by a pronounced infiltration of CD8+T effector cells. This immune-primed landscape enabled BRAFi/MEKi-resistant tumors to exhibit comparable sensitivity to anti-CTLA-4 and anti-PD-1 therapies as their Parental counterparts. Further corroboration in patients with melanoma samples shows that those with elevated EGFR signatures also demonstrate enhanced immune scores, indicative of a potential favorable response to ICI. This congruence between preclinical and clinical data raises the possibility of EGFR as a predictive biomarker, which might be used as a clinical tool to guide therapeutic interventions in patients with melanoma. Hence, our discovery signifies the importance of elucidating resistance mechanisms, as they fundamentally shape the therapeutic trajectory and efficacy of subsequent treatment with ICI.

EGFR upregulation is well recognized as a resistance mechanism to BRAFi/MEKi TT in melanoma. One study found that EGFR was upregulated in 6 out of 16 post-treatment tumor biopsies collected following establishment of resistance.[37] Activation of RTKs, like EGFR, typically triggers the PI3K or MAPK/ERK pathways.[20]

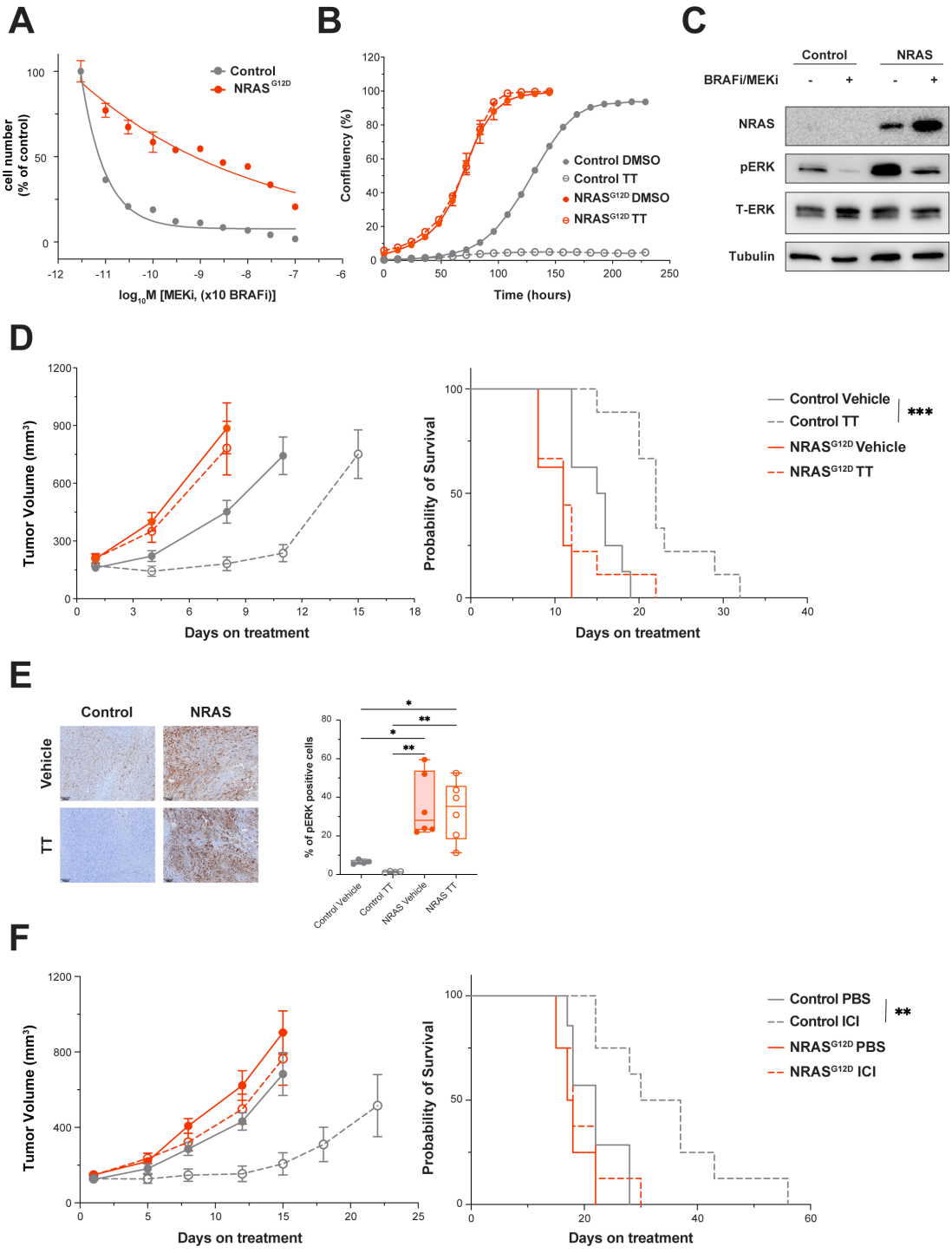

Figure 6 YUMMER 1.7PV1 -NRAS^{G12D} cells are cross-resistant to ICI. (A) Dose response assay of the YUMMER 1.7PV1 cells transduced with empty vector (Control) and NRAS^{G12D}. The dose-response curve is representative of three independent experiments. Error bars show mean±SEM of 5 technical replicates. The cells were treated for 3 days. (B) In vitro proliferation of Control and NRAS^{G12D} cells treated with 50/5 nM of BRAFi/MEKi. Representative of at least three independent experiments, Mean±SEM of 6 technical replicates. (C) Western blot on protein lysates from cells treated for 3 days with the combination of 50 nM of BRAFi and 5 nM of MEKi. A representative of two independent experiments. (D) Tumor volume and survival curves of YUMMER 1.7PV1 Control and NRAS^{G12D} tumors from C57BL/6 mice treated with TT. EV and NRAS Vehicle—n=8 and EV and NRAS BRAFi/MEKi n=9 mice per group. (E) pERK IHC on tumors isolated from C57BL/6 mice after 4 days of BRAFi/MEKi treatment. Scale bar—100 µm. One-way analysis of variance test used for comparison. (F) Tumor volume and survival curve of YUMMER 1.7PV1 Control and NRAS^{G12D} tumors from C57BL/6 mice treated with ICI. EV Vehicle n=7 and EV BRAFi/MEKi, NRAS Vehicle and NRAS BRAFi/MEKi n=8 mice per group. Log-rank (Mantel-Cox) test used for two survival curve comparison. *p<0.05; **p<0.01. BRAFi/MEKi, BRAF/MEK inhibitors; EV, empty vector; ICI, immune checkpoint inhibitors, combination of anti-cytotoxic T lymphocyte antigen-4 and anti-programmed cell death-1 given on day 1, 5 and 9; PBS, phosphate-buffered saline; TT, targeted therapy, combination of BRAFi (dabrafenib) and MEKi (trametinib).

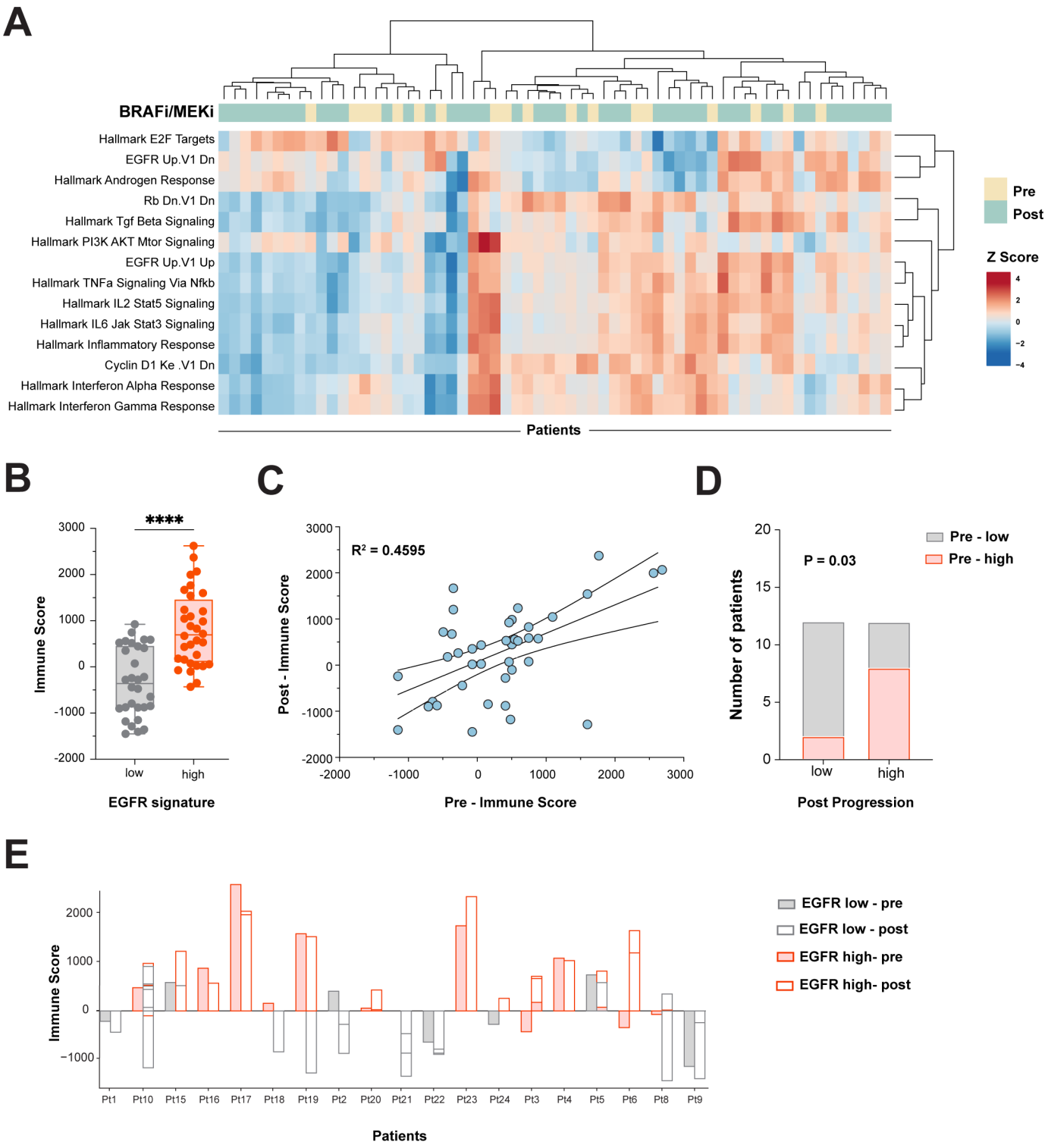

Figure 7 Analysis of patients with melanoma data reveals a correlation between upregulated EGFR gene signature and higher immune scores. (A) Gene Set Variation Analysis score on the patient data set of GSE65185. (B) Immune scores derived with the ESTIMATE algorithm in patients with melanoma with high and low EGFR scores. n=30–32 patients per group; unpaired Mann-Whitney test, ****p<0.0001. (C) Pearson correlation of the immune score obtained in matched pretreatment and post-progression biopsies. (D) A contingency graph illustrating patient with high or low EGFR score at baseline and at post-progression. Fisher's exact test. (E) Side by side comparison of pretreatment and post-treatment biopsies and both their immune score and EGFR signature—refer to supplementary table (online supplemental table S1) for additional details. BRAFi/MEKi, BRAF/MEK inhibitors.

Herein, we demonstrated that in the YR1.7PV1 AR model, resistance was linked to the upregulation of EGFR signaling leading to phosphorylation and activation of STAT3 and STAT5. These findings align with a study by Girotti *et al*,[38] who demonstrated that patients with melanoma develop resistance to BRAFi through upregulation of EGFR-STAT3 signaling. Importantly, in line with our data, they showed that resistance could be reversed with a combination of EGFRi and BRAFi.[38] Another study also showed that BRAFi-resistant cells upregulate STAT3 signaling through RTKs.[39] Consistent with our data, several studies have indicated that the development of resistance through EGFR upregulation is independent of the MAPK/ERK pathway[39 40], validating that our YR1.7PV1 AR model, driven by EGFR-STAT signaling, accurately reflects observations in patients with melanoma. However, while EGFR inhibition alone did not yield a significant antitumor response (figure 5G), this suggests that EGFR inhibition, as a single-agent therapy, may not be sufficient to resensitize tumors to ICI. This underscores the need for further exploration of combination strategies or earlier integration of EGFR-TT in EGFR-STAT-activated tumors.

Acquiring resistance to BRAFi/MEKi via EGFR-STAT signaling maintained ICI sensitivity and was associated with an immune-stimulatory microenvironment. In contrast, the $NRAS^{G12D}$ resistance model with MAPK/ERK pathway overactivation led to ICI cross-resistance. Although $NRAS^{Q61}$ mutations are more prevalent in melanoma, both Q61 and G12D variants similarly activate the MAPK/ERK pathway.[2] Therefore, resistance mechanisms driven by either mutation are likely to exert comparable effects on ICI sensitivity, consistent with previous reports linking MAPK hyperactivation to an immunosuppressive tumor microenvironment.[32] BRAFi/MEKi treatment of EGFR-driven AR melanoma cells led to upregulation of IFN gamma and alpha response gene signatures, including STAT3 and STAT5. Notably, these signatures are established prognostic and predictive markers in stage III melanoma for response to ICI,[41] with elevated STAT3 and STAT5 levels correlating with favorable outcomes to ICI treatment.[42 43] Hyperactivation of STAT3 in tumor cells is associated with increased IL-6 production, which not only contributes to tumorigenesis but also enhances the immune-stimulatory microenvironment.[44] In melanoma, IL-6 upregulation has been linked to poorer clinical outcomes,[45] yet other studies have shown it can alleviate Treg-mediated immune suppression and promote CD8+T cell priming.[46–48] These findings suggest a potential connection between EGFR/STAT3 signaling and enhanced CD8+T cell infiltration in our model. This highlights the role of IL-6 in driving CD8+T cell infiltration, which may have significant implications for improving immunotherapy efficacy. These insights open avenues for future experiments to better understand the relationship between IL-6 and CD8+T cell dynamics, which could ultimately lead to more effective treatment strategies for melanoma and other malignancies.

Of significant clinical relevance is the observation that our BRAFi/MEKi AR model is responsive to ICI therapy when pre-primed with BRAFi/MEKi. This is consistent with observations that elevated CD8+T cell levels[49 50] and the presence of pre-existing intertumoral CD8+T cells are strongly associated with improved progression-free survival and enhanced responses to ICIs in patients.[51] Analysis of patient data sets further supports this, showing a correlation between elevated EGFR signaling and increased antitumor immune cell infiltration. Patients with higher EGFR signatures also exhibit greater immune scores, both pretreatment and post-progression. Matched biopsy analyses reveal that a higher EGFR signature post-progression corresponds to an elevated immune score before and after treatment. Collectively, these findings indicate that patients with upregulated EGFR signatures are more likely to have enhanced immune infiltration and better response to ICIs.

We acknowledge that our findings do not apply to all patients with melanoma, as ICI remains the standard first-line therapy for the majority of patients. However, BRAFi/MEKi continues to play an important role in cases requiring rapid tumor control, such as high disease burden or symptomatic brain metastases. In these contexts, TT as first-line therapy followed by ICI, akin to SECOMBIT-like strategies, remains clinically relevant. Our data suggest that EGFR-STAT activation post-TT could help guide this transition, identifying patients more likely to benefit from an early switch to ICI. To support clinical translation, we propose further investigation to assess the EGFR-STAT activity via immunohistochemistry (IHC) for phosphorylated STAT3 or STAT5 in progression biopsies. While transcriptomic profiling revealed this mechanism in our study, IHC is a more accessible and widely used alternative, offering a practical surrogate for EGFR-STAT signaling. Importantly, the timing and duration of BRAFi/MEKi exposure may critically influence ICI response as prolonged treatment could remodel the tumor microenvironment toward immunosuppression.[8 9 22] Longitudinal studies with pretreatment and post-treatment immune profiling are needed to clarify these dynamics and inform optimal sequencing. Biomarkers like EGFR-STAT activation could aid clinical decision-making, enabling more personalized and effective transitions from TT to ICI.

In conclusion, our findings underscore the critical importance of comprehensively understanding the mechanisms underlying resistance to TT to inform potential sensitivity of second-line ICI. By elucidating the specific pathways involved in TT resistance, such as the EGFR-STAT pathway or the MAPK/ERK pathway, it may be possible to tailor treatment strategies more effectively based on individual patient profiles. As EGFR mutations and hyperactivation of STAT signaling are also common occurrences in other cancer types like colon and lung cancer, our findings may have relevance beyond melanoma.

Author affiliations
[1]Peter MacCallum Cancer Centre, Melbourne, Victoria, Australia
[2]Sir Peter MacCallum Department of Oncology, The University of Melbourne, Melbourne, Victoria, Australia
[3]Olivia Newton-John Cancer Research Institute, Heidelberg, Victoria, Australia
[4]La Trobe University, Melbourne, Victoria, Australia
[5]The Walter and Eliza Hall Institute of Medical Research Melbourne, Melbourne, Victoria, Australia
[6]Department of Medical Biology, University of Melbourne, Melbourne, Victoria, Australia

X Anna S Trigos @anna_t_g

Acknowledgements The authors would like to acknowledge the following core facilities at the Peter MacCallum Cancer Centre: the Molecular Genomics Core (MGC), Flow Cytometry, and the Centre for Advanced Microscopy and Histology. We also extend our gratitude to the members of the Translational Research Laboratory for their assistance with in vivo experiments, with special thanks to Dr Ben Blyth, the laboratory head, and Dr Laura MacPherson, senior scientist, for their invaluable technical guidance.

Contributors RPP, KES, and GAM conceived, conceptualized, and designed the project. Experimental design and supervision were led by RPP, KES, GAM, NH, and AST. Experiments were conducted by RPP, LRJL, RS, DS, and SA. Data analysis was conducted with assistance from MKL and EL. Additional input and support were provided by EL, ADR, and LS, who also contributed critical scientific input, protocols, and/or reagents. RPP drafted the original manuscript, with feedback from all authors. Funding for the study was sourced by KES and GAM. KES is the corresponding author and the guarantor of this manuscript.

Funding This work was supported by grants from the National Health and Medical Research Council of Australia (#2020050 and #2033597) and The Jack and Madeleine Little Foundation. RPP, LRJL, SA, and MKL were supported by doctoral scholarships from the University of Melbourne.

Competing interests None declared.

Patient consent for publication Not applicable.

Ethics approval Not applicable.

Provenance and peer review Not commissioned; externally peer reviewed.

Data availability statement All data relevant to the study are included in the article or uploaded as supplementary information.

ORCID iDs
Riyaben P Patel http://orcid.org/0000-0001-8916-0307
Lydia Rui Jia Lim http://orcid.org/0000-0002-4031-7809
Reem Saleh http://orcid.org/0000-0002-8292-1895
Aparna D Rao http://orcid.org/0000-0002-6394-0011
Lorey Smith http://orcid.org/0000-0001-6130-978X
Anna S Trigos http://orcid.org/0000-0002-5915-2952
Karen E Sheppard http://orcid.org/0000-0002-2798-4703

REFERENCES

1 Robert C, Grob JJ, Stroyakovskiy D, *et al*. Five-Year Outcomes with Dabrafenib plus Trametinib in Metastatic Melanoma. *N Engl J Med* 2019;381:626–36.
2 Ribas A, Daud A, Pavlick AC, *et al*. Extended 5-Year Follow-up Results of a Phase Ib Study (BRIM7) of Vemurafenib and Cobimetinib in *BRAF*-Mutant Melanoma. *Clin Cancer Res* 2020;26:46–53.
3 Larkin J, Chiarion-Sileni V, Gonzalez R, *et al*. Five-Year Survival with Combined Nivolumab and Ipilimumab in Advanced Melanoma. *N Engl J Med* 2019;381:1535–46.
4 Begley J, Ribas A. Targeted therapies to improve tumor immunotherapy. *Clin Cancer Res* 2008;14:4385–91.
5 Pelster MS, Amaria RN. Combined targeted therapy and immunotherapy in melanoma: a review of the impact on the tumor microenvironment and outcomes of early clinical trials. *Ther Adv Med Oncol* 2019;11:1758835919830826.
6 Kuske M, Westphal D, Wehner R, *et al*. Immunomodulatory effects of BRAF and MEK inhibitors: Implications for Melanoma therapy. *Pharmacol Res* 2018;136:151–9.
7 Liu C, Peng W, Xu C, *et al*. BRAF inhibition increases tumor infiltration by T cells and enhances the antitumor activity of adoptive immunotherapy in mice. *Clin Cancer Res* 2013;19:393–403.
8 Song C, Piva M, Sun L, *et al*. Recurrent Tumor Cell-Intrinsic and -Extrinsic Alterations during MAPKi-Induced Melanoma Regression and Early Adaptation. *Cancer Discov* 2017;7:1248–65.
9 Frederick DT, Piris A, Cogdill AP, *et al*. BRAF inhibition is associated with enhanced melanoma antigen expression and a more favorable tumor microenvironment in patients with metastatic melanoma. *Clin Cancer Res* 2013;19:1225–31.
10 Gutzmer R, Stroyakovskiy D, Gogas H, *et al*. Atezolizumab, vemurafenib, and cobimetinib as first-line treatment for unresectable advanced BRAFV600 mutation-positive melanoma (IMspire150): primary analysis of the randomised, double-blind, placebo-controlled, phase 3 trial. *The Lancet* 2020;395:1835–44.
11 Ferrucci PF, Di Giacomo AM, Del Vecchio M, *et al*. KEYNOTE-022 part 3: a randomized, double-blind, phase 2 study of pembrolizumab, dabrafenib, and trametinib in *BRAF*-mutant melanoma. *J Immunother Cancer* 2020;8:e001806.
12 Ascierto PA, Mandalà M, Ferrucci PF, *et al*. Sequencing of Ipilimumab Plus Nivolumab and Encorafenib Plus Binimetinib for Untreated *BRAF*-Mutated Metastatic Melanoma (SECOMBIT): A Randomized, Three-Arm, Open-Label Phase II Trial. *J Clin Oncol* 2023;41:212–21.
13 Atkins MB, Lee SJ, Chmielowski B, *et al*. Combination Dabrafenib and Trametinib Versus Combination Nivolumab and Ipilimumab for Patients With Advanced *BRAF*-Mutant Melanoma: The DREAMseq Trial-ECOG-ACRIN EA6134. *J Clin Oncol* 2023;41:186–97.
14 Boutros A, Croce E, Ferrari M, *et al*. The treatment of advanced melanoma: Current approaches and new challenges. *Crit Rev Oncol Hematol* 2024;196:104276.
15 Hugo W, Shi H, Sun L, *et al*. Non-genomic and Immune Evolution of Melanoma Acquiring MAPKi Resistance. *Cell* 2015;162:1271–85.
16 Wagle N, Van Allen EM, Treacy DJ, *et al*. MAP kinase pathway alterations in BRAF-mutant melanoma patients with acquired resistance to combined RAF/MEK inhibition. *Cancer Discov* 2014;4:61–8.
17 Whittaker SR, Theurillat J-P, Van Allen E, *et al*. A Genome-Scale RNA Interference Screen Implicates NF1 Loss in Resistance to RAF Inhibition. *Cancer Discov* 2013;3:350–62.
18 Shi H, Hong A, Kong X, *et al*. A novel AKT1 mutant amplifies an adaptive melanoma response to BRAF inhibition. *Cancer Discov* 2014;4:69–79.
19 Czarnecka AM, Bartnik E, Fiedorowicz M, *et al*. Targeted Therapy in Melanoma and Mechanisms of Resistance. *Int J Mol Sci* 2020;21:4576.
20 Wang J, Huang SK, Marzese DM, *et al*. Epigenetic changes of EGFR have an important role in BRAF inhibitor-resistant cutaneous melanomas. *J Invest Dermatol* 2015;135:532–41.
21 Müller J, Krijgsman O, Tsoi J, *et al*. Low MITF/AXL ratio predicts early resistance to multiple targeted drugs in melanoma. *Nat Commun* 2014;5:5712.
22 Pieper N, Zaremba A, Leonardelli S, *et al*. Evolution of melanoma cross-resistance to $CD8^+$ T cells and MAPK inhibition in the course of BRAFi treatment. *Oncoimmunology* 2018;7:e1450127.
23 Luebker SA, Koepsell SA. Diverse Mechanisms of BRAF Inhibitor Resistance in Melanoma Identified in Clinical and Preclinical Studies. *Front Oncol* 2019;9:268.
24 Wang J, Perry CJ, Meeth K, *et al*. UV-induced somatic mutations elicit a functional T cell response in the YUMMER1.7 mouse melanoma model. *Pigment Cell Melanoma Res* 2017;30:428–35.
25 Meeth K, Wang JX, Micevic G, *et al*. The YUMM lines: a series of congenic mouse melanoma cell lines with defined genetic alterations. *Pigment Cell Melanoma Res* 2016;29:590–7.
26 Ritchie ME, Phipson B, Wu D, *et al*. limma powers differential expression analyses for RNA-sequencing and microarray studies. *Nucleic Acids Res* 2015;43:e47.

27 Wu T, Hu E, Xu S, *et al*. clusterProfiler 4.0: A universal enrichment tool for interpreting omics data. *Innovation (Camb)* 2021;2:100141.
28 Castanza AS, Recla JM, Eby D, *et al*. Extending support for mouse data in the Molecular Signatures Database (MSigDB). *Nat Methods* 2023;20:1619–20.
29 Hänzelmann S, Castelo R, Guinney J. GSVA: gene set variation analysis for microarray and RNA-seq data. *BMC Bioinformatics* 2013;14:7.
30 Sturm G, Finotello F, List M. Immunedeconv: An R Package for Unified Access to Computational Methods for Estimating Immune Cell Fractions from Bulk RNA-Sequencing Data. *Methods Mol Biol* 2020;2120:223–32.
31 Yoshihara K, Shahmoradgoli M, Martínez E, *et al*. Inferring tumour purity and stromal and immune cell admixture from expression data. *Nat Commun* 2013;4:2612.
32 Haas L, Elewaut A, Gerard CL, *et al*. Acquired resistance to anti-MAPK targeted therapy confers an immune-evasive tumor microenvironment and cross-resistance to immunotherapy in melanoma. *Nat Cancer* 2021;2:693–708.
33 Zhong Z, Wen Z, Darnell JE. Stat3 and Stat4: members of the family of signal transducers and activators of transcription. *Proc Natl Acad Sci USA* 1994;91:4806–10.
34 Liu X, Robinson GW, Gouilleux F, *et al*. Cloning and expression of Stat5 and an additional homologue (Stat5b) involved in prolactin signal transduction in mouse mammary tissue. *Proc Natl Acad Sci USA* 1995;92:8831–5.
35 Nazarian R, Shi H, Wang Q, *et al*. Melanomas acquire resistance to B-RAF(V600E) inhibition by RTK or N-RAS upregulation. *Nature New Biol* 2010;468:973–7.
36 Heidorn SJ, Milagre C, Whittaker S, *et al*. Kinase-dead BRAF and oncogenic RAS cooperate to drive tumor progression through CRAF. *Cell* 2010;140:209–21.
37 Sun C, Wang L, Huang S, *et al*. Reversible and adaptive resistance to BRAF(V600E) inhibition in melanoma. *Nature New Biol* 2014;508:118–22.
38 Girotti MR, Pedersen M, Sanchez-Laorden B, *et al*. Inhibiting EGF receptor or SRC family kinase signaling overcomes BRAF inhibitor resistance in melanoma. *Cancer Discov* 2013;3:158–67.
39 Vultur A, Villanueva J, Krepler C, *et al*. MEK inhibition affects STAT3 signaling and invasion in human melanoma cell lines. *Oncogene* 2014;33:1850–61.
40 Kwong LN, Boland GM, Frederick DT, *et al*. Co-clinical assessment identifies patterns of BRAF inhibitor resistance in melanoma. *J Clin Invest* 2015;125:1459–70.
41 Versluis JM, Blankenstein SA, Dimitriadis P, *et al*. Interferon-gamma signature as prognostic and predictive marker in macroscopic stage III melanoma. *J Immunother Cancer* 2024;12:e008125.
42 Hossain SM, Gimenez G, Stockwell PA, *et al*. Innate immune checkpoint inhibitor resistance is associated with melanoma subtypes exhibiting invasive and de-differentiated gene expression signatures. *Front Immunol* 2022;13:955063.
43 Xie Y, Zhang J, Li M, *et al*. Identification of Lactate-Related Gene Signature for Prediction of Progression and Immunotherapeutic Response in Skin Cutaneous Melanoma. *Front Oncol* 2022;12:818868.
44 Chang Q, Bournazou E, Sansone P, *et al*. The IL-6/JAK/Stat3 feed-forward loop drives tumorigenesis and metastasis. *Neoplasia* 2013;15:848–62.
45 Hoejberg L, Bastholt L, Schmidt H. Interleukin-6 and melanoma. *Melanoma Res* 2012;22:327–33.
46 Sharma MD, Hou D-Y, Baban B, *et al*. Reprogrammed foxp3(+) regulatory T cells provide essential help to support cross-presentation and CD8(+) T cell priming in naive mice. *Immunity* 2010;33:942–54.
47 Böttcher JP, Schanz O, Garbers C, *et al*. IL-6 trans-signaling-dependent rapid development of cytotoxic CD8+ T cell function. *Cell Rep* 2014;8:1318–27.
48 McLoughlin RM, Jenkins BJ, Grail D, *et al*. IL-6 trans-signaling via STAT3 directs T cell infiltration in acute inflammation. *Proc Natl Acad Sci USA* 2005;102:9589–94.
49 Andrews MC, Duong CPM, Gopalakrishnan V, *et al*. Gut microbiota signatures are associated with toxicity to combined CTLA-4 and PD-1 blockade. *Nat Med* 2021;27:1432–41.
50 Edner NM, Ntavli E, Petersone L, *et al*. Stratification of PD-1 blockade response in melanoma using pre- and post-treatment immunophenotyping of peripheral blood. *Immunother Adv* 2023;3:ltad001.
51 Tumeh PC, Harview CL, Yearley JH, *et al*. PD-1 blockade induces responses by inhibiting adaptive immune resistance. *Nature New Biol* 2014;515:568–71.